ARTICLE

Trimetallic MOF-Derived CoFeNi/Z-P NC Nanocomposites as efficient catalysts for oxygen evolution reaction

Received 00th January 20xx,
Accepted 00th January 20xx

DOI: 10.1039/x0xx00000x

Xudun Shen[a], Liping Huang[a], Shuaishuai Li[a], Longnian Tang[a], Qiemei Lei[a], Bowang Zhao[a], Huilian Hao[a], Wenyao Li[a,c*], Min Zeng[b,*] and Guanjie He[c,*]

We used sodium hydroxide-mediated approach and tannic acid etching to prepare hollow structure trimetallic MOF-derived CoFeNi/Z-P NC Nanocomposites. Remarkably, the resulting CoFeNi/Z-P NC have large specific surface area and mesoporous structure, making their active sites more accessible and makes mass transfer more effective. More complex trimetallic components provide more possibilities for further improving electrocatalytic performance. The CoFeNi/Z-P NC nanocomposites demonstrate a notable enhancement for the OER, 10 mA cm^{-2} current density is achieved at a low overpotential 244 mV, with a low tafel slope of 66.2 mV dec^{-1} and has good stability for alkaline solutions. In addition, as a cathode material for overall alkaline water splitting, CoFeNi/Z-P NC is better than RuO_2 along with long cycling stability.

1. Introduction

Due to its critical role in numerous energy conversion and storage technologies, the oxygen evolution reaction (OER) has attracted a lot of attention as a study issue in recent years [1-4]. However, the OER's slow kinetics and multielectron transfer process make it challenging to use in practical applications because the reaction requires a significant overpotential to drive it [5, 6]. The remarkable catalytic efficacy of noble metal catalysts, such as RuO_2 and IrO_2, in promoting the OER, is widely known, but their high cost and limited availability severely restrict their widespread practical usage [7, 8]. Therefore, to deal with the OER, it is vital to create efficient and long-lasting alternative electrocatalysts [9, 10].

With the aim of resolving this issue, the nanostructured transition metal phosphides (TMPs) were recognized as promising candidates for catalysts in the oxygen evolution reaction (OER), and important developments have been achieved in this area [11-13]. However, these catalysts based on transition metal phosphides still need to perform better in the OER. According to studies, controlling the structure and chemical composition of transition metal-based electrocatalysts is necessary to increase their intrinsic OER activity [14, 15]. The first includes changing the structure to promote mass transportation and increase the exposure of the active location [16]. Given this, hollow-structured nanoporous materials that have gained a lot of attention include those that have a large specific surface area, lots of active sites, and short charge transfer distances [17, 18]. The latter part entails purposeful modification of stoichiometric compositions to control the electrical characteristics, affecting interactions with reaction intermediates and reaction dynamics as a result [19]. Consequently, internal or phase interface engineering has emerged as a viable strategy for controlling the electrical properties [20]. In their bimetallic phosphides made from MOF precursors, Chen et al. showed that a Ni_2P/CoP contact was essential for producing a synergistic effect and boosting the electrocatalytic activity [21]. However, due to the highly intricate chemical composition of transition metal phosphides, even slight variations in the metal-to-phosphorus stoichiometric ratio can result in substantial alterations in their structures. As a result, there is a scarcity of studies concentrating on combining hollow structures with various transition metal phosphides.

Zhang et al.[22] synthesized NiCoP/NC PHCs by using bimetal as precursor and combining tannic acid-induced chemical corrosion with subsequent roasting and phosphating. The obtained composite material has a good hollow structure. Hong et al.[23] developed a very simple sodium hydroxide-mediated method to prepare Fe-Co bimetallic MOFs with high yields. However, there are currently few methods for doping two other metals into ZIF-67 to form trimetallic ZIFs, and there are even fewer studies on hollow trimetallic MOFs and their derivatives.

In this study, we synthesized trimetallic CoFeNi-ZIF specimens by incorporating iron and nickel dopants into ZIF-67. Then we used tannic acid as an etchant to perform in-situ chemical etching on the cobalt-based trimetallic zeolite imidazole framework polyhedron (CoFeNi-ZIF), forming a hollow-structured CoFeNi-Z. Subsequently, two steps of carbonization and phosphating were carried out. The as-synthesized CoFeNi/Z-P NC nanocomposite exhibits a distinctive hollow structure and benefits from the coordinating impact arising from the uniform integration of metallic Fe and Ni. These nanocomposites display a low overpotential of 244 mV at a current density of 10 mA cm^{-2} due to increased electrocatalytic activity for OER. Additionally, as a cathode material for overall alkaline water electrolysis, CoFeNi/Z-P NC is better than RuO_2 along with long cycling stability.

2. Experimental

2.1 Chemical

2-Methylimidazole (Adamas, 98%), Sodium hydroxide (aladdin, 97%), Cobalt nitrate hexahydrate (Shanghai Lingfeng Chemical Reagent Co., Ltd., ⩾99%), Iron (III) chloride hexahydrate (Greagent, 99%), Nickel nitrate hexahydrate (Greagent, ⩾98.5%), and Sodium

[a] School of Materials Science and Engineering, Shanghai University of Engineering Science, Shanghai 201620, China.
[b] Department of Micro/Nano Electronics, School of Electronic Information and Electrical Engineering, Shanghai Jiao Tong University, 800 Dong Chuan Road, Shanghai, 200240, PR China.
[c] Electrochemical Innovation Lab, Department of Chemical Engineering, University College London, London, WC1E 7JE, UK.
*Corresponding author, E-mail: liwenyao314@gmail.com; minzeng@sjtu.edu.cn; g.he@ucl.ac.uk

hypo-phosphite monohydrate (Wuxi Yatai United Chemical Co., Ltd., 99%). All of chemicals have been used as received.

2.2 Synthesis of CoFeNi/ZIF

By using the bimetallic synthesis technique described in the earlier literature, CoFeNi-ZIF is synthesized. In a typical synthesis, 5 mL 1 M aqueous solution of sodium hydroxide was combined with a 5 mL 3.36 M aqueous solution of 2-methylimidazole under stirring, forming solution A. For the preparation of solution B, a 0.446 mL 0.8 M aqueous solution of cobalt nitrate and a 0.223 mL 0.8 M aqueous solution of nickel nitrate were mixed with a 1.78 mL 0.1 M aqueous solution of iron trichloride, and the volume was adjusted to 6 mL with deionized water. Subsequently, solution B was slowly added to solution A using a pipette. The reaction proceeded for 3 hours at a stirring rate of 400 rpm. The final product was obtained by centrifugation at an acceleration of 8000 rpm, collected, and dried at 60 ℃ for additional use after being three times methanol washed. CoFe-ZIF and CoNi-ZIF compounds were synthesised using similar techniques.

2.3 Synthesis of CoFeNi/Z

In a typical synthesis, 1.25 g of tannic acid and 250 mL of methanol were combined with 0.5 g of the previously synthesised CoFeNi-ZIF compound. The mixture was spun for 5 minutes at a speed of 300 rpm. The finished product was then recovered by centrifugation at an acceleration of 8000 rpm, dried at 60 ℃ for further uses after being thrice cleaned in methanol and deionized water.

2.4 Synthesis of CoFeNi/Z-P NC

The dried CoFeNi-Z material was loaded into a ceramic boat and placed into a temperature-controlled furnace. The furnace's temperature was gradually increased from 20 ℃ to 700 ℃ at a heating rate of 10 ℃ min^{-1}, and it was then kept there for two hours. Subsequently, the furnace was let cool off on its own to room temperature. Throughout the entire process, a continuous flow of pure argon gas was employed. The resulting product was designated as CoFeNi/Z NC.

Place the as-prepared CoFeNi/Z NC and $NaH_2PO_2 \cdot H_2O$ at a mass ratio of 1:10 downstream and upstream in the tube furnace. A The sample was then heated to 400 ℃ at an average rate of 5 ℃ min^{-1} and maintained there for two hours under Ar atmosphere. After cooling to room temperature, a phosphide product called CoFeNi/Z-P NC was obtained and further utilized.

3.Results and Discussion

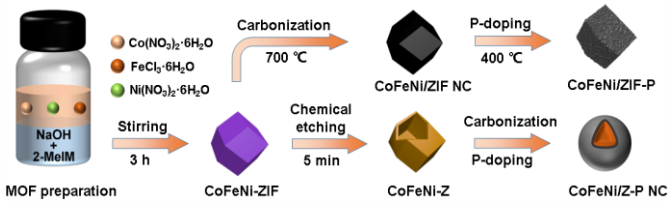

Fig. 1 Schematic diagram of the synthesis of materials.

Fig. 1 shows a schematic representation of the CoFeNi/Z-P NC ternary alloy synthesis process. In a typical synthesis, the raw materials were added to an aqueous sodium hydroxide and 2-methylimidazole mixture, which quickly changed the mixture's colour to purple. This reaction yielded metal-organic framework (MOF) precursors referred to as CoFeNi-ZIF hereafter. For comparison, CoFe-ZIF and CoNi-ZIF samples were also prepared (Fig. S1†). The XRD pattern of the CoFe-ZIF and CoNi-ZIF samples exhibited similarities to that of CoFeNi-ZIF (Fig. S2†) and analysis using energy-dispersive X-rays (EDS) confirmed the elemental species of CoFeNi-ZIF (Fig. S3†).

Tannic acid is used as the etching agent in in situ chemical etching to convert CoFeNi-ZIF into CoFeNi-Z (step 2 in Fig. 1). It takes 5 minutes to complete the process. The etching reaction induced by tannic acid is a surface functionalization-assisted etching process. Tannic acid provides protons to destroy the coordination bonds of CoFeNi-ZIF, causing the disintegration of the MOF. At the same time, tannic acid can be adsorbed on the surface of CoFeNi-ZIF to protect the MOF. not etched[24]. SEM and TEM were employed to illustrate the unique structure and morphology of the sample (Fig. S4† and Fig. S5 †). The color change from CoFeNi-ZIF to CoFeNi-Z also confirms the evolution of the structure (Fig. S6†), which is consistent with our previous findings [22]. CoFeNi/ZIF-P can be obtained by direct carbonization of CoFeNi-ZIF and then phosphating. CoFeNi-Z is first carbonized and then phosphorized to obtain CoFeNi/Z-P NC. CoFeNi/ZIF NC and CoFeNi/Z NC are obtained by direct carbonization of CoFeNi-ZIF and CoFeNi-Z under argon atmosphere.

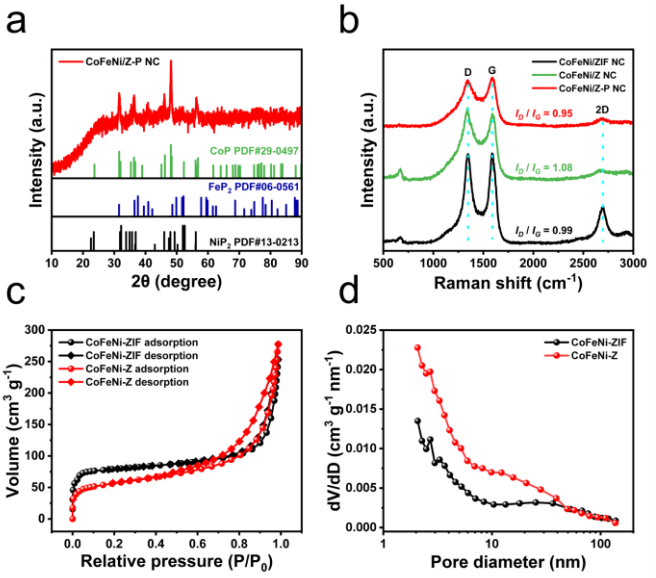

Fig. 2 (a) The XRD of CoFeNi/Z-P NC are shown. (b) The Raman spectra of CoFeNi/ZIF NC, CoFeNi/Z NC, and CoFeNi/Z-P NC. (c) The nitrogen adsorption-desorption isotherms of CoFeNi-ZIF and CoFeNi-Z. (d) The pore size distribution of CoFeNi-ZIF and CoFeNi-Z.

X-ray diffraction, Raman spectroscopy, and BET tests were also carried out to determine the chemical state of the sample and to disclose the synergistic impact of various metal phosphides. CoFeNi/Z-P NC alloy particle X-ray diffraction (XRD) pattern is shown in Fig. 2a. The diffraction peaks of CoP (PDF#29-0497), FeP_2 (PDF#06-0561), and NiP_2 (PDF#13-0213) appeared in CoFeNi/Z-P NC, indicating that the crystalline phases of CoP, FeP_2, and NiP_2 were formed [23, 25, 26]. The D band and G band, which are represented by the Raman spectrum's two unique peaks at 1351 and 1596 cm^{-1}, respectively. 2D band peak was also observed at 2703 cm^{-1} [27]. While the G bands come from in-plane sp^2 carbon vibrations, the D bands come from sp^2 carbon imperfections. Additionally we noticed weaker 2D bands indicating the presence of graphene-like carbon sheets in the material [28]. The calculated intensity ratio of I_D/I_G is 0.99, 1.08, and 0.95 for CoFeNi/ZIF NC, CoFeNi/Z NC, and CoFeNi/Z-P NC electrocatalysts, respectively. The high I_D/I_G ratio indicates the generation of numerous defects, implying significant doping of the graphene layer with heterogeneous atoms [29]. Additionally, the larger and weaker 2D bands suggest that the alloy has thin graphene layers on it. BET analysis confirms some evolution of material structure

(Fig.2c and Fig.2d), demonstrating that the CoFeNi-Z material has a specific surface area of 270.138 $m^2 g^{-1}$, the typical pore size is 8.885 nm, and a total volume of pores of 0.429 $cm^3 g^{-1}$. Comparatively, CoFeNi-ZIF has a surface area of 361.033 $m^2 g^{-1}$, a pore size of 6.022 nm on average, and a total volume of pores of 0.392 $cm^3 g^{-1}$. This further confirms the impact of etching on the material structure.

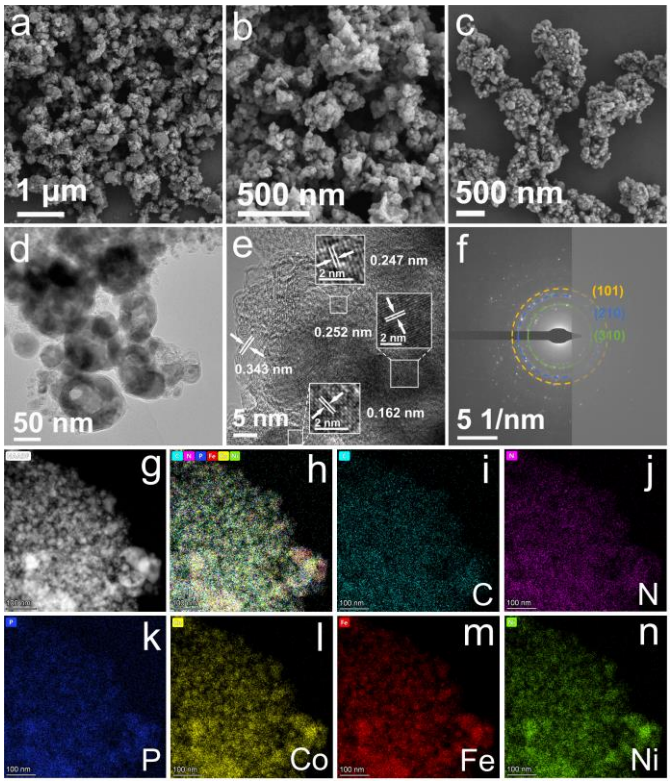

Fig. 3 (a, b, and c) SEM images of CoFeNi-ZIF, CoFeNi-Z, and CoFeNi/Z-P NC. (d) TEM images of CoFeNi/Z-P NC. (e) HRTEM image of CoFeNi/Z-P NC. (f) SAED pattern of CoFeNi/Z-P NC. (g-n) STEM image and elemental mappings of CoFeNi/Z-P NC.

Fig. 3a shows the SEM image of CoFeNi-ZIF. It can also be seen that it is a dodecahedron between 50-100 nm. Fig. 3b shows the scanning electron microscope image of CoFeNi-Z, the morphology of the sample after in situ etching has changed, the surface is rough and more irregular than before. Fig. 3c showcases the morphology of CoFeNi/Z-P NC. The transmission electron microscope (TEM) image in Fig. 3d confirms the sample's hollow structure, and it also clearly shows the N-doped graphene shell and the number of layers of graphene is approximately 5 to 10. The Supporting Information contains higher resolution HRTEM images of the hollow structure (Fig.S7†). The (200), (200), and (310) planes of FeP_2, CoP, and NiP_2 are depicted in the high-resolution TEM (HRTEM) image as lattice fringes with d-spacing values of approximately 0.247 nm, 0.252 nm, and 0.162 nm [30], respectively, which closely match the expected spacing values (Fig. 3e). A polycrystalline structure can be seen in the CoFeNi/Z-P NC selected area electron diffraction (SAED) pattern (Fig. 3f), as evident from the diffraction rings. High-angle annular dark-field scanning electron microscopy (HAADF-STEM) (Fig. 3g), which shows differential properties in the inner and outer portions, further confirms a core-shell structure for the nanocrystals. And analysis using energy-dispersive X-rays (EDS) confirmed the elemental species of CoFeNi/Z-P (Fig. S8†).

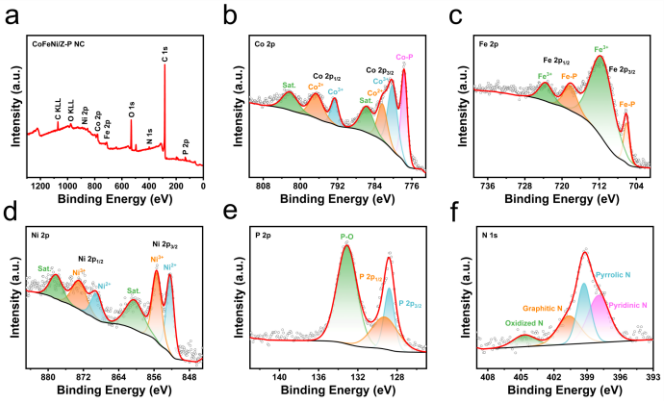

Fig. 4 XPS spectra of CoFeNi/Z-P NC. (a) Survey scan. (b) Co 2p. (c) Fe 2p. (d) Ni 2p. (e) P 2p and (f) N 1s peaks of CoFeNi/Z-P NC.

Analysis of CoFeNi/Z-P NC samples with the use of X-ray photoelectron spectroscopy (XPS) revealed important information about their chemical composition and bonding states. On the surface of CoFeNi/Z-P NC, the whole XPS spectrum in Fig. 4a verifies the existence of C, N, P, and transition metal ions Co, Fe, and Ni [31]. According to the Co 2p spectra (Fig. 4b), the first pair identified at 780.18 eV (Co $2p_{3/2}$) and 792.58 eV (Co $2p_{1/2}$) are compatible with Co in the Co^{2+} oxidation state. The second set of lines, which are located at 782.38 eV ($Co2p_{3/2}$) and 796.68 eV ($Co2p_{1/2}$), indicate the existence of Co^{3+} species. For the peaks at 785.88 eV and 802.48 eV, shakeup satellites are to blame. Additionally, the emergence of a unique spinorbit peak at 777.78 eV provides further evidence that Co-P bonds were produced in the CoFeNi/Z-P NC sample [32, 33]. The peaks at 706.18 eV (Fe $2p_{2/3}$) and 718.38 eV (Fe $2p_{1/2}$), as well as 711.88 eV (Fe $2p_{2/3}$) and 723.68 eV (Fe $2p_{1/2}$), in the Fe 2p spectra (Fig. 4c), are indicative of Fe-P bonds. Peaks represent Fe-O surface bonds[34]. The Ni 2p XPS spectrum (Fig. 4d) reveals the detailed electronic states of Ni_2P compound , exhibiting four spin-orbit peaks along with two satellite peaks labeled as "Sat.". The existence of both Ni^{2+} and Ni^{3+} species is indicated by peaks at 852.38 eV and 855.38 eV, which are followed by peaks at 869.18 eV and 873.18 eV, respectively [35, 36]. A pair of peaks at 128.78 eV and 129.28 eV, attributed to P $2p_{3/2}$ and P $2p_{1/2}$, respectively, in the high-resolution P 2p spectrum (Fig. 4e), suggest the formation of metal phosphides. Peaks at 133.08 eV suggest that sample oxidation in the air caused the formation of P-O bonds [37, 38]. Pyridinic nitrogen (397.98 eV), pyrrolic nitrogen (399.28 eV), graphitized nitrogen (400.68 eV), and nitrogen oxide (404.68 eV) were the four peaks seen in the N 1s spectrum (Fig. 4f) [39, 40]. The electrocatalytic activity is significantly impacted by both pyridinic-N and graphitic-N species, it is vital to highlight [41, 42].And Tab. S1† shows the chemical compositions of CoFeNi/Z-P NC by XPS measurement.

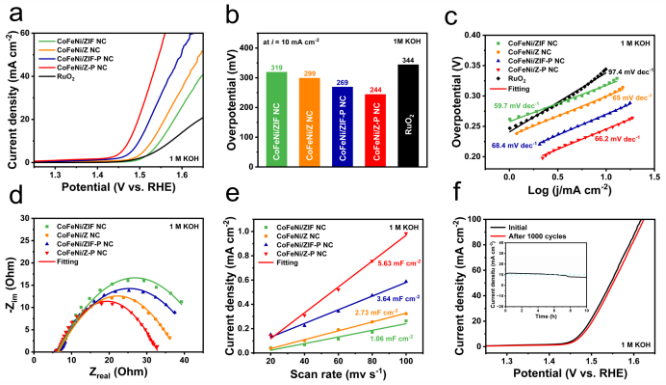

Fig. 5 (a) Polarization curves and (b) overpotential performance. Tafel slopes (c) and EIS Nyquist plots (d). (e)The non-Faradaic region of CV curves was fitted to obtain information about the double-layer capacitance. (f) The durability test was conducted by measuring the polarization curves of CoFeNi/Z-P NC before and after the test, with the chronoamperometry measurement performed at 1.48 V for 10 hours (the inset).

The catalytic performance of the catalyst for the oxygen evolution reaction (OER) was assessed using a typical three-electrode electrochemical cell device in a 1M potassium hydroxide solution. The counter electrode was a graphite rod, while the reference electrode was a saturated Ag/AgCl electrode. LSV assessed the samples' OER activity and compared it to a RuO_2 electrocatalyst used as a commercial benchmark. The LSV curves in Fig. 5a demonstrate the excellent performance of the CoFeNi/Z-P NC catalyst, which has an overpotential of 244 mV at a current density of 10 mA $cm^{-2.}$ Compared to the values presented in Fig. 5b for RuO_2 (344 mV), CoFeNi/ZIF NC (319 mV), CoFeNi/Z NC (299 mV), and CoFeNi/ZIF-P NC (269 mV), this value was much lower. The Tafel slope is then obtained by fitting the linear component of the Tafel diagram with the Tafel equation ($\eta = b\log j + a$), where b is the Tafel slope and j is the current density. RuO_2 has a value of 97.4 mV dec^{-1} on the Tafel slopes in Fig. 5c, which is consistent with the theoretical value. Compared to CoFeNi/ZIF NC, CoFeNi/Z, and CoFeNi/ZIF-P NC, which had Tafel slopes of 59.7 mV dec^{-1}, 65 mV dec^{-1}, and 68.4 mV dec^{-1}, respectively, CoFeNi/Z-P NC had a measured Tafel slope of 66.2 mV dec^{-1}. We compare the OER electrocatalytic performance of the obtained catalyst with different catalysts (Tab. S2†). At the same time, we compared the RuO_2 parameter obtained from the experiment with the literature (Tab. S3†). The Nyquist plots in Fig. 5d indicate that CoFeNi/Z-P NC exhibited smaller semicircle diameters compared to CoFeNi/ZIF NC, CoFeNi/Z NC, and CoFeNi/ZIF-P NC, suggests a decreased charge transfer resistance at the catalyst/electrolyte contact. A decreased charge transfer resistance denotes greater electrode material conductivity, which is generally recognised to be connected to electrocatalysis kinetics.

Furthermore, cyclic voltammetry was used to quantify the electrochemical double-layer capacitance (C_{dl}), which is thought to be directly proportional to the electrochemical active surface area (ECSA). The CV curves for F CoFeNi/ZIF NC, CoFeNi/Z NC, CoFeNi/ZIF-P NC, and CoFeNi/Z-P NC in the non-Faradaic area are shown in Fig. S8 at various scan rates (20, 40, 60, 80, and 100 mV s^{-1}). As depicted in Fig. 5e, the calculated C_{dl} value for CoFeNi/Z-P NC is 5.63 mF cm^{-2}, surpassing that of CoFeNi/ZIF NC (1.06 mF cm^{-2}), CoFeNi/Z NC (2.73 mF cm^{-2}), and CoFeNi/ZIF-P NC (3.64 mF cm^{-2}). With only a slight decline in current density over a 10-hour period, Fig. 5f and the inset show the CoFeNi/Z-P NC's strong durability. After this step we collected the sample and performed TEM test (Fig. S10†). The graphene shell is clearly visible and the lattice parameters correspond to those before testing (Fig.3e).

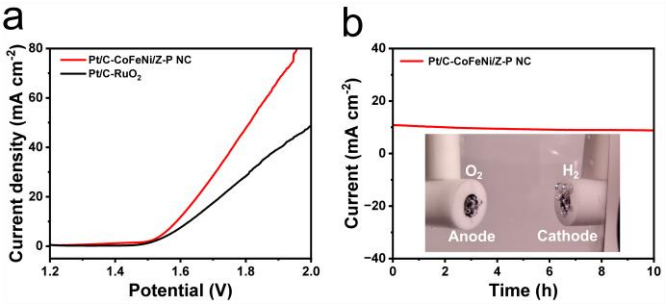

Fig. 6 (a) Polarization curves of Pt/C-CoFeNi/Z-P NC and Pt/C-RuO_2 catalyst couples for overall water splitting in 1.0 M KOH. (b) Time-dependent current density curves (i-t curve) under static overpotentials of 1.59V in 1.0 M KOH. The inset is an optical photograph showing the generation of H_2 and O_2 bubbles for Pt/C- CoFeNi/Z-P NC on glassy carbon electrode.

As shown in Fig. 6a, a current density of 10 mA cm^{-2} could be achieved by applying a potential of 1.588 V between two electrodes, which is even smaller than that of its Pt-RuO_2 counterpart (1.627 V). The very stable current density at a high potential of 1.59 V in i–t curves (Fig. 6b) further demonstrated the strong stability of CoFeNi/Z-P NC. The negligible activity of carbon paper further proved the activity came from the catalysts. The excellent activity of the alloy catalyst, accompanied by high stability, made it a potential alternative for precious catalysts in practical water splitting.

4. Conclusion

In summary, this study presents an efficient catalyst CoFeNi/Z-P NC, derived from CoFeNi trimetallic hollow MOF phosphides through a combination of MOF derivation, *in situ* etching, and phosphating techniques. CoFeNi/Z-P NC exhibits effective catalytic synergy for the electrochemical OER. Structural transformation of CoFeNi-ZIF to hollow CoFeNi-Z derivatives as well as phosphides observed by physical characterization. The CoFeNi/Z-P NC sample, which demonstrates increased catalytic activity for OER, only needs 244 mV of overpotential to achieve a current density of 10 mA cm^{-2} on a glassy carbon electrode. It has a low tafel slope of 66.2 mV dec^{-1} and excellent stability, and we have expanded the application of CoFeNi/Z-P NC in total water splitting. This work introduces a new preparation method of trimetallic hollow MOFs and extends their applications in energy conversion and catalytic reactions.

Supplementary data

Supplementary data include the characterization instrument model of the sample, the method of electrochemical measurement, and the synthesis process diagram of the sample and the SEM, TEM, XRD, EDS and other information of the comparative samplems.

Conflicts of interest

There are no conflicts to declare.

Acknowledgements

This work was financially supported by the National Natural Science Foundation of China (Grant No. 62374107), The Talent Program of Shanghai University of Engineering Science (QNTD202104), Shanghai Local Universities Capacity Building Project of Science and Technology Innovation Action Program (21010501700), Class III Peak Discipline of Shanghai-Materials

Science and Engineering (High-Energy Beam Intelligent Processing and Green Manufacturing).

Reference

1. R. Liu, S. Xu, X. Shao, Y. Wen, X. Shi, L. Huang, M. Hong, J. Hu and Z. Yang, ACS Appl. Mater. Interfaces, 2021, 13, 47717-47727.
2. X. Gu, Y. G. Ji, J. Tian, X. Wu and L. Feng, Chem. Eng. J., 2022, 427, 131576.
3. F. Li, J. Li, L. Zhou and S. Dai, Sustainable Energy Fuels, 2021, 5, 1095-1102.
4. J. Song, C. Wei, Z. F. Huang, C. Liu, L. Zeng, X. Wang and Z. J. Xu, Chem. Soc. Rev., 2020, 49, 2196-2214.
5. Z. Qin and J. Zhao, J. Colloid Interface Sci., 2022, 605, 155-162.
6. J. Yu, Q. He, G. Yang, W. Zhou, Z. Shao and M. Ni, ACS Catal., 2019, 9, 9973-10011.
7. L. Tian, Z. Li, M. Song and J. Li, Nanoscale, 2021, 13, 12088-12101.
8. L. Zhang, H. Jang, H. Liu, M. G. Kim, D. Yang, S. Liu, X. Liu and J. Cho, Angew. Chem. Int. Edit., 2021, 60, 18821-18829.
9. X. R. Wang, J. Y. Liu, Z. W. Liu, W. C. Wang, J. Luo, X. P. Han, X. W. Du, S. Z. Qiao and J. Yang, Adv. Mater., 2018, 30, 1800005.
10. N. T. Suen, S. F. Hung, Q. Quan, N. Zhang, Y. J. Xu and H. M. Chen, Chem. Soc. Rev., 2017, 46, 337-365.
11. Y. Wang, B. Kong; D. Y. Zhao; H. T. Wang; C. Selomulya, Nano Today, 2017, 15, 26-55.
12. C. Wu, Y. Yang, D. Dong, Y. Zhang and J. Li, Small, 2017, 13, 1602873.
13. Z. Pu, T. Liu, I. S. Amiinu, R. Cheng, P. Wang, C. Zhang, P. Ji, W. Hu, J. Liu and S. Mu, Adv. Funct. Mater., 2020, 30, 2004009.
14. Q. Shao, P. Wang and X. Huang, Adv. Funct. Mater., 2019, 29, 1806419.
15. Q. Kang, D. Lai, W. Tang, Q. Lu and F. Gao, Chem. Sci., 2021, 12, 3818-3835.
16. I. S. Amiinu, Z. Pu, X. Liu, K. A. Owusu, H. G. R. Monestel, F. O. Boakye, H. Zhang and S. Mu, Adv. Funct. Mater., 2017, 27, 1702300.
17. J. Yang, F. Zhang, H. Lu, X. Hong, H. Jiang, Y. Wu and Y. Li, Angew. Chem. Int. Edit., 2015, 54, 10889-10893.
18. Z. F. Huang, J. Song, K. Li, M. Tahir, Y. T. Wang, L. Pan, L. Wang, X. Zhang and J. J. Zou, J. Am. Chem. Soc., 2016, 138, 1359-1365.
19. X. Zheng, Y. Zhang, H. Liu, D. Fu, J. Chen, J. Wang, C. Zhong, Y. Deng, X. Han and W. Hu, Small, 2018, 14, 1803666.
20. Y. Li, Z. Dong and L. Jiao, Adv. Energy Mater., 2019, 10, 1902104.
21. X. Liang, B. Zheng, L. Chen, J. Zhang, Z. Zhuang and B. Chen, ACS Appl. Mater. Interfaces, 2017, 9, 23222-23229.
22. X. Zhang, L. Huang, Q. Wang and S. Dong, J. Mater. Chem. A, 2017, 5, 18839-18844.
23. W. Hong, M. Kitta and Q. Xu, Small Methods, 2018, 2, 1800214.
24. M. Hu, Y. Ju, K. Liang, T. Suma, J. Cui and F. Caruso, Adv. Funct. Mater., 2016, 26, 5827-5834.
25. L. Han, M. Zhang, H. Wang, P. Li, W. Wei, J. Shi, M. Huang, Z. Shi, W. Liu and S. Chen, Nanoscale, 2020, 12, 24477-24487.
26. G. Zhang, Y. Li, X. Xiao, Y. Shan, Y. Bai, H. G. Xue, H. Pang, Z. Tian and Q. Xu, Nano Lett., 2021, 21, 3016-3025.
27. J. Qiao, X. Kong, Z. X. Hu, F. Yang and W. Ji, Nat. Commun., 2014, 5, 4475.
28. L. Huang, W. Li, X. Shen, C. Sun, J. Yang, X. Shi and M. Zeng, J. Mater. Chem. A, 2022, 10, 7111-7121.
29. J. Deng, P. Ren, D. Deng and X. Bao, Angew. Chem. Int. Edit., 2015, 54, 2100-2104.
30. M. Zhang, T. Wang, H. Cao, S. Cui and P. Du, J. Energy Chem., 2020, 42, 71-76.
31. J. G. Li, H. Sun, L. Lv, Z. Li, X. Ao, C. Xu, Y. Li and C. Wang, ACS Appl. Mater. Interfaces, 2019, 11, 8106-8114.
32. R. Xiang, Y. Duan, C. Tong, L. Peng, J. Wang, S. S. A. Shah, T. Najam, X. Huang and Z. Wei, Electrochim. Acta, 2019, 302, 45-55.
33. X. Liu, G. He, H. Liu, Y. Zhu, J. Xiao and L. Han, J. Alloys Compd., 2022, 893, 162208.
34. H. J. Niu, S. Y. Lin, Y. P. Chen, J. J. Feng, Q. L. Zhang and A. J. Wang, Appl. Surf. Sci., 2021, 536, 147950.
35. J. Cao, R. Zhao, L. Bai, Y. Wang, Z. Zhang, L. Wu, X. Du and J. Li, Appl. Surf. Sci., 2023, 627, 157287.
36. X. Chen, H. Tao, Y. Jiang, S. Li, Y. Liu, K. Xie and Y. Wang, J. Energy Storage, 2023, 68, 107721.
37. M. Yao, H. Hu, N. Wang, W. Hu and S. Komarneni, J. Colloid Interface Sci., 2020, 561, 576-584.
38. Z. Liu, M. Wang, X. Luo, S. Li, S. Li, Q. Zhou, W. Xu and R. Wu, Appl. Surf. Sci., 2021, 544, 148912.
39. Q. Shi, Q. Liu, Y. Ma, Z. Fang, Z. Liang, G. Shao, B. Tang, W. Yang, L. Qin and X. Fang, Adv. Energy Mater., 2020, 10, 1903854.
40. Z. Peng, H. Wang, X. Xia, X. Zhang and Z. Dong, ACS Sustainable Chem. Eng., 2020, 8, 9009-9016.
41. J. Q. Chi, W. K. Gao, J. H. Lin, B. Dong, K. L. Yan, J. F. Qin, B. Liu, Y. M. Chai and C. G. Liu, ChemSusChem, 2018, 11, 743-752.
42. G. Yan, X. Feng, S. U. Khan, L. Xiao, W. Xi, H. Tan, Y. Ma, L. Zhang and Y. Li, Chem-Asian J, 2018, 13, 158-163.